Bulletin of Earthquake Engineering (2018) 16:5171–5193
https://doi.org/10.1007/s10518-018-0409-6

ORIGINAL RESEARCH

Comparison between cyclic and dynamic rocking behavior for embedded shallow foundation using centrifuge tests

Kil-Wan Ko[1] · Jeong-Gon Ha[1] · Heon-Joon Park[1] · Dong-Soo Kim[1]

Received: 6 September 2017 / Accepted: 12 June 2018 / Published online: 21 June 2018

Abstract
Designs allowing the rocking behavior of the foundation during earthquake have been introduced to reduce the seismic load on the superstructure and the ductility demand on the structural column. In addition, several studies have been conducted on rocking foundation based on the slow cyclic and dynamic tests by assuming the structure as a rigid oscillator. However, when structural bending is included, the rocking behaviors of the foundation for the slow cyclic and dynamic tests are different. Therefore, a clear description of each method and how each behavior is different should be investigated by considering structural bending motion. To fill the gap between cyclic and dynamic rocking behaviors, embedded foundation models with various slenderness ratios of the systems were investigated using horizontal slow cyclic tests and dynamic tests in a centrifuge. Test results show that the rocking foundation was affected by structural bending. The overturning moment in the dynamic test determined by the conventional method was different compared with results obtained from the slow cyclic test due to the structural bending motion. Finally, the overturning moment was re-evaluated by considering structural net displacement, and the re-evaluated dynamic overturning moment matched the results from the slow cyclic tests.

Keywords Rocking foundation · Embedded shallow foundation · Single-degree-of-freedom structure · Horizontal slow cyclic test · Dynamic centrifuge test

✉ Dong-Soo Kim
dskim@kaist.ac.kr

Kil-Wan Ko
kwko@kaist.ac.kr

Jeong-Gon Ha
jgha87@kaist.ac.kr

Heon-Joon Park
heonjoon@kaist.ac.kr

[1] Department of Civil and Environmental Engineering, Korea Advanced Institute of Science and Technology (KAIST), 291 Daehakro, Yuseong-gu, Daejeon 34141, Republic of Korea

1 Introduction

Considering soil-foundation-structure interaction (SFSI) in seismic design enables structures to be constructed efficiently and precisely. In particular, the design method of allowing the rocking behavior of the foundation during earthquake has been introduced as an effective seismic design to reduce the seismic load on the superstructure and the ductility demand on the structural column. Since the rocking behavior of the foundation can be allowed by reducing the bearing capacity of the foundation, applying the rocking behavior of the foundation called "rocking foundation" or "rocking isolation" has the advantage of not only seismic load reduction on the superstructure but also economical seismic design. Despite the benefits of the rocking foundation method, it is not easy to apply in practice owing to lack of understanding of the rocking behavior concept and difficulty in controlling the permanent deformation induced by the rocking behavior.

To overcome the deficiency of lack of understanding of the rocking mechanism, many studies have been conducted using numerical and experimental techniques. To evaluate the rocking foundation, most studies were conducted using the slow cyclic test (Negro et al. 2000; Gajan and Kutter 2009a, b; Anastasopoulos et al. 2011, 2012; Gazetas et al. 2013; Kokkali et al. 2014, 2015; Liu et al. 2015b; Hakhamaneshi and Kutter 2016), or the dynamic test (Combescure and Chaudat 2000; Mergos and Kawashima 2005; Paolucci et al. 2008; Anastasopoulos et al. 2010; Deng et al. 2012; Heron et al. 2013; Liu et al. 2013; Anastasopoulos et al. 2013, 2014; Heron et al. 2015; Allmond and Kutter 2014; Kim et al. 2015; Liu et al. 2015c; Tsatsis and Anastasopoulos 2015; Figini and Paolucci 2017; Pelekis et al. 2017), or both test methods (Gajan et al. 2005; Gajan and Kutter 2008; Shirato et al. 2008; Hung et al. 2011; Deng and Kutter 2012; Drosos et al. 2012; Gelagoti et al. 2012; Panagiotidou et al. 2012; Gazetas 2015; Liu et al. 2015a). Pecker et al. (2014) presented an overview of recent researches on non-linear dynamic SFSI using experimental test. For the slow cyclic test, horizontal cyclic loading is applied directly at the top of the structure; therefore, this test is an effective technique for observing ground deformation caused by slow cyclic loading at the top of the structure. On the other hand, the dynamic test (such as the shaking table test) can evaluate the seismic load on the superstructure and predict the soil–foundation–structure behavior in practice. However, most studies designed the structural model as a rigid oscillator such that the structure would not be bent during slow cyclic and dynamic tests (Gajan et al. 2005; Gajan and Kutter 2008; Anastasopoulos et al. 2012; Drosos et al. 2012; Anastasopoulos et al. 2013; Kokkali et al. 2014). There are two reasons for designing the structural model as a rigid oscillator. One is related to the objective of the rocking foundation design. Since the objective of the rocking foundation is to protect the structure during earthquake by allowing soil–foundation yielding, the behavior of the structure should be within the elastic range. The other reason is to easily compare the foundation–structure behavior during slow cyclic and dynamic tests. For the slow cyclic test, the flexural displacement of the structure will be negligible even if it occurs owing to the longer period of cyclic loading compared to the structural natural period. Therefore, the experiment for rocking foundation models a structure as a rigid oscillator. Gajan et al. (2005) stated that the overturning moment–rotation backbone curve of the foundation obtained from the slow cyclic test results can predict the dynamic rocking behavior of a shallow foundation using the rigid structural model. However, in practice, even if the rocking foundation concept was used, structural bending would be generated during earthquake due to the resonance effect. Therefore, the gap between the slow cyclic and the dynamic rocking behaviors of the system with structural bending should be investigated in detail. In

addition, to improve understanding of the experimental approach to rocking foundation, it is necessary to evaluate a method to analyze the dynamic rocking behavior with structural bending.

Meanwhile, attempts to apply the rocking foundation concept in practice have persisted (Paolucci et al. 2013; Deng et al. 2014; Hakhamaneshi et al. 2016; Kutter et al. 2016). Since the performance of a structure is related to the displacement of the structure, the direct displacement-based design (DDBD) is regarded as an appropriate design method for rocking foundation, and the requirement of structural displacement during earthquake can be effectively reduced by the foundation rocking behavior. In particular, to apply the DDBD method in practice, Deng et al. (2014) used a trilinear backbone curve and a multilinear hysteretic model for the overturning moment–rotation relation determined from the slow cyclic and dynamic centrifuge tests. Since both the slow cyclic and the dynamic tests have been used to determine the applicability of rocking foundation in practice, it is necessary to investigate the difference between the slow cyclic and dynamic tests with structural bending. Finally, understanding the difference between the dynamic and slow cyclic rocking behaviors with structural bending can make rocking foundation design closer to practical application.

The objectives of this study are to investigate the difference between the cyclic and dynamic behaviors, and to fill the gap of understanding between the cyclic and dynamic behaviors of embedded rocking foundations by considering structural bending. Since the effective stiffness of the structure changes according to its height, the slenderness ratio of the structure (i.e., ratio of height of the structure to the foundation length) and the structural stiffness should be considered simultaneously. Both the slow cyclic and dynamic shaking table tests were conducted with three different slenderness ratios of structures with embedded foundation system. The overturning moment for slow cyclic and dynamic tests was determined using a load cell attached to a horizontal actuator and accelerometer on the structure, respectively. The foundation rotation angle for slow cyclic and dynamic tests was measured using two displacement sensors (linear variable differential transformer (LVDT)) and two accelerometers oppositely placed at the end of the foundation, respectively. The overturning moment and rotation curves obtained from the slow cyclic and dynamic tests with embedded rocking foundation were compared. By considering the foundation horizontal, rocking, and structural bending motions, the dynamic overturning moment were evaluated in detail. The results are useful in terms of filling the gap between the cyclic and dynamic behaviors of embedded rocking foundations with moment–rotation backbone curve.

2 Discussion on slow cyclic and dynamic rocking behaviors for embedded foundation–structure system by considering structural bending

As shown in Fig. 1, during earthquake, the horizontal displacement at the top of the structure is decomposed into three parts: foundation horizontal displacement, horizontal displacement due to foundation rocking, and structural net displacement. By considering the structural motion, as well as the foundation and soil behavior during earthquake, a general equation for the dynamic motion of a single degree of freedom (SDOF) structure considering SFSI can be expressed as follows (Tileylioglu et al. 2011; Kim et al. 2015):

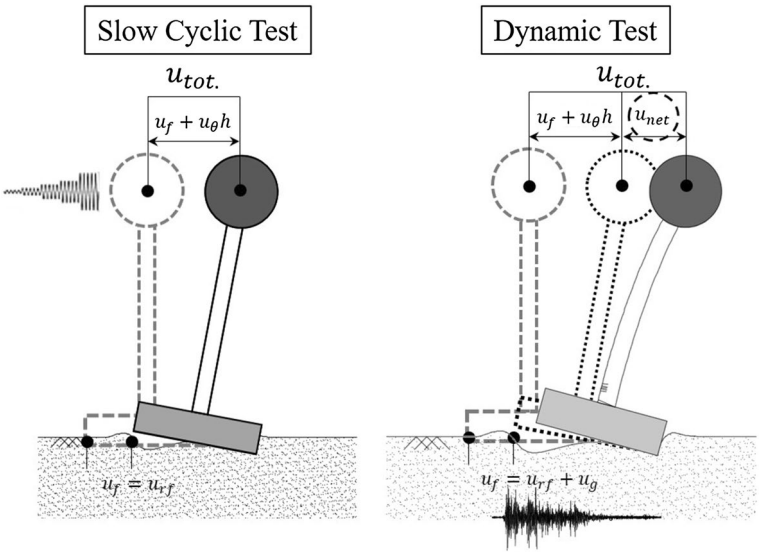

Fig. 1 Slow cyclic and dynamic response of SDOF structure considering SFSI

$$\begin{bmatrix} m_s & m_s & m_s h \\ m_s & m_s + m_f & m_s h \\ m_s h & m_s h & m_s h^2 + I_f \end{bmatrix} \begin{bmatrix} \ddot{u}_{net} \\ \ddot{u}_{rf} \\ \ddot{u}_\theta \end{bmatrix} + \begin{bmatrix} c_s & 0 & 0 \\ 0 & c_f & 0 \\ 0 & 0 & c_\theta \end{bmatrix} \begin{bmatrix} \dot{u}_{net} \\ \dot{u}_{rf} \\ \dot{u}_\theta \end{bmatrix} + \begin{bmatrix} k_s & 0 & 0 \\ 0 & k_f & 0 \\ 0 & 0 & k_\theta \end{bmatrix} \begin{bmatrix} u_{net} \\ u_{rf} \\ u_\theta \end{bmatrix} = - \begin{bmatrix} m_s \\ m_s + m_f \\ m_s h \end{bmatrix} \ddot{u}_g \tag{1}$$

where m_s is the effective mass of the structure; m_f is the foundation mass; I_f is the rotational moment of inertia of the foundation; c_s is the structural damping coefficient; c_f and c_θ are the damping coefficient of sliding and rocking of the foundation, respectively; k_s is the effective stiffness of the structure; k_f and k_θ are the sliding and rocking stiffness of the foundation, respectively; h is the effective height of the structure; u_{net} and u_g are the horizontal displacement of structural bending and soil, respectively; u_{rf} is the horizontal relative displacement between the foundation and soil; and u_θ is the rotation angle of the foundation. The third row of Eq. 1 indicates the rocking behavior of the entire system. Since the rotational moment of inertia of the foundation is smaller than $m_s h^2$, the term I_f can be neglected. Equation 1 can be arranged as follows:

$$M_o \approx -k_\theta u_\theta = m_s h\left(\ddot{u}_{net} + \ddot{u}_f + h\ddot{u}_\theta\right) + c_\theta \dot{u}_\theta = m_s h\left(\ddot{u}_{tot.}\right) + c_\theta \dot{u}_\theta \tag{2}$$

where M_o is the overturning moment of the foundation; $\ddot{u}_f$ is the horizontal acceleration of the foundation ($\ddot{u}_f = \ddot{u}_g + \ddot{u}_{rf}$); and $\ddot{u}_{tot.}$ is the total acceleration of the horizontal motion of the structure ($\ddot{u}_{tot.} = \ddot{u}_{net} + \ddot{u}_f + \ddot{u}_\theta h$). The accelerometer attached to the structure measures the total acceleration of the horizontal motion of the structure ($\ddot{u}_{tot.}$). Although the contribution of the rotational damping of the foundation ($c_\theta \dot{u}_\theta$) can affect the overturning moment of the foundation, the horizontal motion of the structure ($\ddot{u}_{tot.}$) mainly contributes to the overturning moment of the foundation (Gajan and Kutter 2008). Therefore, the dynamic overturning moment can be easily determined using the mass of the structure (m_s), the effective height (h), and the total acceleration of the horizontal motion of the structure ($\ddot{u}_{tot.}$).

However, when the structure behaves like a rigid oscillator, the overturning moment of the foundation is determined only by foundation sliding and rocking motion, which can be expressed as

$$M_{ro} \approx -k_\theta u_\theta = m_s h\left(\ddot{u}_f + h\ddot{u}_\theta\right) + c_\theta \dot{u}_\theta = m_s h\left(\ddot{u}_{f\_tot.}\right) + c_\theta \dot{u}_\theta \tag{3}$$

where M_{ro} is the overturning moment of the foundation for a rigid oscillator structure and $\ddot{u_{f\_tot.}} = \ddot{u}_f + h\ddot{u}_\theta$. Although the total acceleration of the structure ($\ddot{u}_{f\_tot.}$) mainly affects the overturning moment (M_{ro}), if the structure is rigid, the total acceleration of the structure does not include the acceleration of the structural bending ($\ddot{u}_{net}$) during the earthquake. In addition, in the slow cyclic test, the long period of cyclic loading is too far from the natural period of the structure to generate significant structural bending motion. Consequently, by modeling the structure as a rigid oscillator, the overturning moment of the foundation during slow cyclic tests can predict the dynamic overturning moment of the foundation. However, as expressed in Eq. 2, the structural bending motion should be generated during dynamic motion, and in this case, the overturning moment of the foundation during slow cyclic tests does not closely match the dynamic overturning moment. Therefore, in this study, a method to deal with the structural bending motion (u_{net}) was investigated and its effects were observed in order to compare the slow cyclic and dynamic overturning moments.

3 Centrifuge testing program

Centrifuge tests were conducted to replicate stress conditions of soil in the field. The tests were conducted with a centrifuge at the KOCED Geotechnical Centrifuge Testing Center at KAIST (Kim et al. 2013a). The centrifugal acceleration for the tests was 20 g-level, and the model description and interpretation of test results were expressed as a prototype scale applied to a scaling law (Madabhushi 2014). In the dynamic tests, an in-flight earthquake simulator below the soil box simulates earthquake motion. The loading frequency range of the earthquake simulator at KAIST was 40–300 and 40–200 Hz for random vibration and sinusoidal wave, respectively; other specifications of the earthquake simulator are described in Kim et al. (2013b).

3.1 Structural modeling

The structural models were formed into a SDOF structure having a lumped mass at the top of the structure (Fig. 2). Fukui et al. (1999) stated that typical slenderness ratios of highway bridge pier range from 0.5 to 2.0; to observe the different governing behaviors of foundations such as sliding or rocking, the SDOF structural models have different slenderness ratios, 1 (ST4), 1.5 (ST8), and 2 (ST12). The slenderness ratio (h/L) of the structure is the ratio of the effective height (h) of the test models, which is the ratio of the height of the effective mass (m_s) as a point mass to the foundation length (L). The slow cyclic and dynamic tests were conducted using the same models. To facilitate cyclic loading of the structural models, the top of the structural model was U-shaped.

To evaluate the dynamic behavior of a foundation–structure model, specifically the dynamic overturning moment, the effective mass (m_s) and the effective stiffness (k_s) of the structural model should be determined accurately. As shown in Fig. 2b–d, to obtain the effective mass and the effective stiffness of a structural model, impact hammer tests were

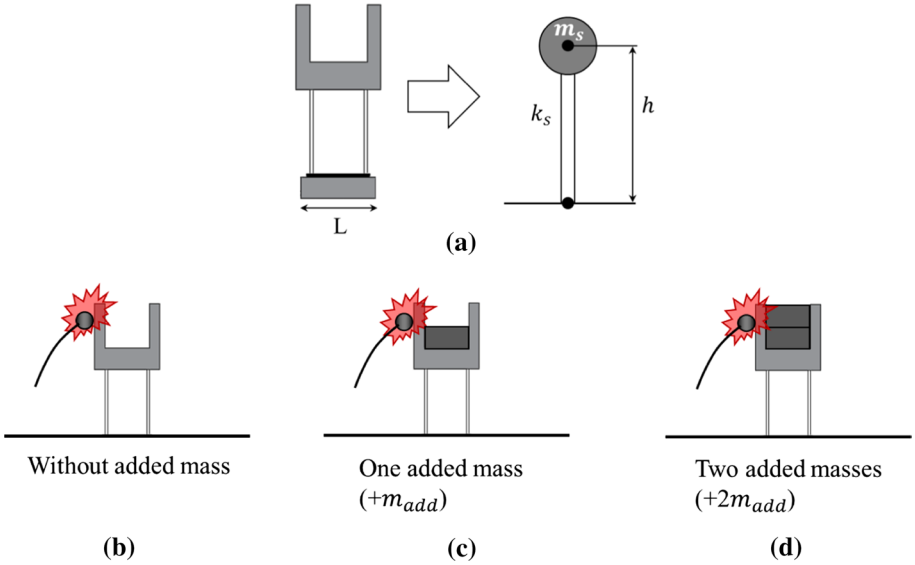

Fig. 2 Schematic diagram of a structural model: **a** idealized SDOF structural model; **b**, **c**, and **d** are the impact hammer tests on the fixed-base structural model without added mass, with one added mass, and two added masses, respectively

conducted with a fixed base condition at 1 g-level state. Using the natural frequency of the structural model at each test (i.e., Figure 2b without added mass, Fig. 2c with one added mass), the effective mass and the effective stiffness were calculated as follows:

$$f_n = \frac{1}{2\pi}\sqrt{\frac{k_s}{m_s}}, \quad f_{n\_add} = \frac{1}{2\pi}\sqrt{\frac{k_s}{m_s + m_{add}}} \tag{4}$$

where f_n is the natural frequency of the structural model without added mass (m_{add}), and f_{n_add} is the natural frequency of the structural model with added mass. To validate the obtained m_s and k_s values, the impact hammer test for the structural model with two added masses was conducted (Fig. 2d). The effective mass and the effective stiffness of the structural model were validated by comparing the measured and calculated natural frequency of the structural model with two added masses.

3.2 Ground modeling

Dry Saemangeum sand—natural sand that contains high fine contents—was used to develop the ground model. The basic soil properties are listed in Table 1. A rectangular model box and an equivalent shear beam (ESB) box were used to conduct the slow cyclic and dynamic tests, respectively. The ESB box reduced the boundary effect during dynamic tests (Lee et al. 2013). The dimensions of the rectangular model box were 99.5×99.5×47.5 cm (length×width×height), and the dimensions of the ESB box were 49×49×63 cm (length×width×height). To model the soil at the target relative density of 40%, the soil

Table 1 Properties of the ground model

Property	Saemangeum sand Slow cyclic/dynamic
Soil model properties	
Unified soil classification (USCS)	SM
Coefficient of uniformity (C_u)	2.11
Mean grain size, D_{50} (mm)	0.08
Soil thickness (mm)	200/500
Dry density, ρ_d (t/m^3)	1.3
Relative density, D_r (%)	40
Friction angle	37.3
Prototype properties	
Centrifugal acceleration (g)	20
Soil thickness (m)	4/10

weight corresponding to the volume of each model box was calculated, and the soil layer was divided into four sublayers for the rectangular model box and five sublayers for the ESB box.

Rocking foundation has advantages of reducing the structural ductility demand and the seismic load on the superstructure; Kim et al. (2015) stated that the seismic load on the superstructure is restricted to the ultimate moment capacity of the foundation (M_{ult}). In contrast, owing to plastic hinging in soil, permanent deformation (e.g., settlement and rotation) is a problem for rocking foundation design. For practical application of rocking foundation, a balance should be achieved between the reduction of seismic load on a structure and permanent deformation in soil. Gajan and Kutter (2008) stated that the critical contact area ratio, the ratio of the foundation area (A) to the critical contact area (A_c) (i.e., the minimum area to support the vertical load), is related to the ultimate moment capacity, energy dissipation, and permanent deformation. In addition, Gajan and Kutter (2008) suggested that $A/A_c = 10$ is an appropriate value of rocking foundation to establish a balance between energy dissipation in soil and permanent deformation. Consequently, the dimensions of the foundation model were determined as 1.4 × 1.4 × 0.4 m (length × width × height) with $A/A_c = 10$. In addition, the foundation model was made into an aluminum foundation with a weight of 2 tons in prototype scale, and the mass of the aluminum foundation was much smaller than that of the structural model. The foundation model was identically used for each test model.

To obtain accurate vertical bearing capacity of the foundation and critical contact area ratio (A/A_c), the vertical load test was conducted on a shallow foundation model of the Saemangeum sand with relative density of 40% at 20 g—the same condition for the cyclic and dynamic tests. The measured vertical factor of safety (FS_v) and the critical contact area ratio (A/A_c) were approximately 11. The friction angle of the soil was back-calculated using the Meyerhof (1963) equation. Details of the ground model are described in Ko et al. (2018). Table 2 summarizes the basic properties of the test models.

Table 2 Properties of the test model [prototype scale (model scale)]

Model names	ST4	ST8	ST12
Effective mass (m_s)	15.8 ton (1.98 kg)	18.9 ton (2.36 kg)	18.3 ton (2.29 kg)
Effective height (h)	1.4 m (70 mm)	2.1 m (105 mm)	2.8 m (140 mm)
Footing length (L)	1.4 m (70 mm)	1.4 m (70 mm)	1.4 m (70 mm)
Slenderness ratio (h/L)	1	1.5	2
Effective stiffness, k_s (kN/m)	49,362 kN/m (2468 kN/m)	11,616 kN/m (580.8 kN/m)	3656 kN/m (182.8 kN/m)
Natural frequency (f_n)	8.9 Hz (178 Hz)	3.9 Hz (78 Hz)	2.3 Hz (46 Hz)
Natural period (T_n)	0.11 s (0.0055 s)	0.25 s (0.0125 s)	0.44 s (0.022 s)
Embedment depth	0.4 m (20 mm)	0.4 m (20 mm)	0.4 m (20 mm)
Critical contact area ratio (A/A_c)	11.9	11.6	11.3
Vertical factor of safety (FS_v)	11.6	11.3	11.1

3.3 Slow cyclic and dynamic centrifuge tests

3.3.1 Slow cyclic tests

Horizontal slow cyclic tests were conducted by displacement control. Identical cyclic displacement protocol was applied to each test model. The toppling displacement (δ_R) for a rigid oscillator on a rigid base is half of the foundation length ($L/2$, 0.7 m). Twenty-five cycles (5 cycles at each amplitude, 5, 10, 20, 30, and 50% of δ_R) were applied to the top of the structure. To avoid the inertial force of the structure, the period of cyclic loading was determined as 50 s on the model scale.

Figure 3a shows the experimental setup and the sensor arrangement for the slow cyclic tests. The height of the ground model was 4 m in the prototype scale, which is 2.8 times the length of the foundation, and the embedment depth was 0.4 m, the same as the height of the foundation. The cover, which fits into the structural models for applying cyclic loading, allows the test model to deform freely during the cyclic test and a load cell was placed between the horizontal actuator and the cover. Horizontal loads measured by the load cell were used to calculate the applied overturning moment of the foundation by considering the $P-\delta$ effect. In addition, the two LVDT sensors were installed with the same distance as the foundation length for determining the rotation angle of the foundation. The rotation angle was determined by the inverse tangent ($\tan^{-1}$) value of the ratio ($\left(L_1 - L_2\right)/L$)), that is, the ratio of the difference of the LVDT values ($L_1 - L_2$) to the foundation length (L). Details of the slow cyclic tests are described in Ko et al. (2018).

3.3.2 Dynamic tests

Figure 3b shows the test setup and the sensor arrangement for the dynamic tests. The height of the ground model was 10 m in the prototype scale, which is 7.1 times the length of the

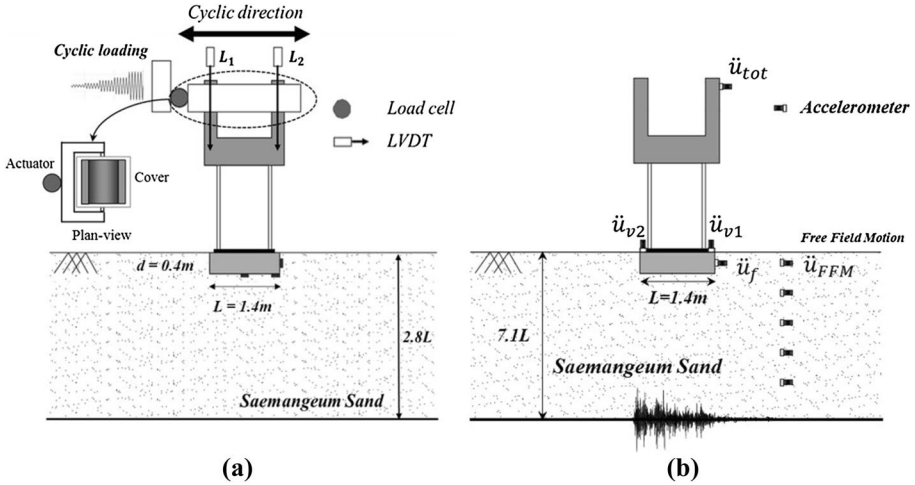

Fig. 3 Sectional view of the centrifuge test setup: **a** slow cyclic tests (Ko et al. 2018); **b** dynamic tests (Ko et al. 2017)

foundation, and the foundation embedment depth was 0.4 m, the same as the height of the foundation. An accelerometer was used to measure the acceleration of each part in the dynamic test. The horizontal displacements of the structure ($u_{tot.}$) and the foundation (u_f) were obtained by double integration of the accelerations signal. To investigate the dynamic rotation of the foundation, the difference in the vertical displacement ($u_{v1} - u_{v2}$) at the edge of the foundation obtained by double integration of the acceleration signals was divided by the foundation length (L), then the foundation rotation angle was determined by the inverse tangent ($\tan^{-1}$) value of the ratio ($(u_{v1} - u_{v2})/L$). The horizontal acceleration at the soil surface was measured as free-field motion ($\ddot{u}_{FFM}$).

Figure 4 shows the normalized acceleration time histories and response spectrum of the input motions for the dynamic centrifuge tests. Each test model was subjected to sweep signal, which has energy in various freqeucny ranges, and real earthquake recorded motions. To investigate the frequency characteristics of the soil, foundation, and structural system, sweep

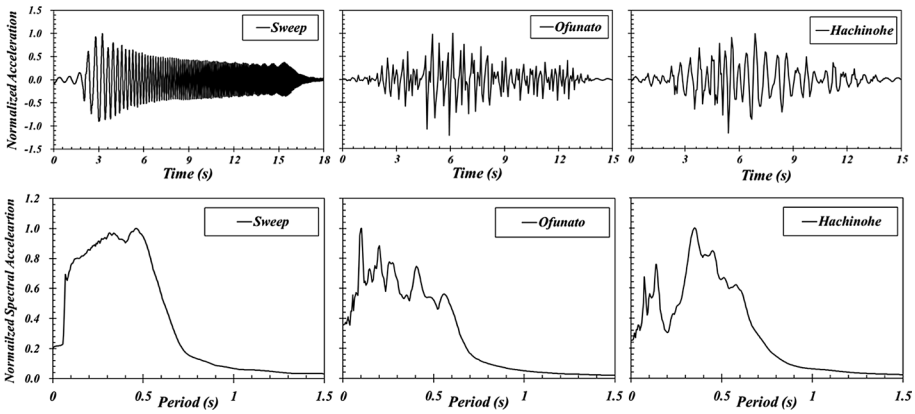

Fig. 4 Normalized acceleration time histories and response spectrum of input motions

Table 3 Sequence of the dynamic loading and peak input acceleration for the dynamic centrifuge tests (unit: g)

Sequence of the earthquake	ST4	ST8	ST12
Sweep	0.03–0.05	0.03–0.05	0.03–0.05
Ofunato (initial)	0.50	0.34	0.51
Hachinohe (initial)	0.37	0.33	0.37
Ofunato (stage)	0.02–0.37	0.02–0.33	0.03–0.35
Hachinohe (stage)	0.03–0.39	0.04–0.33	0.04–0.32
Number of earthquakes	32	27	33

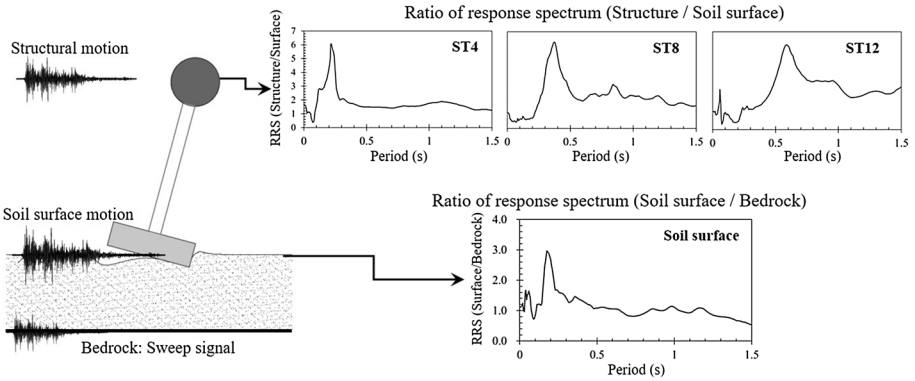

Fig. 5 Ratio of response spectrum (RRS) of soil surface and structure during the weak sweep signal

signal was applied as base motion. Ofunato earthquake motions, which represent short period dominated earthquake signals, and Hachinohe earthquake motions, which represent long period dominated earthquake signals, were used as input base motions. Initially, weak sweep signal was applied to the test models, then, strong earthquake signals were applied using Ofunato and Hachinohe earthquake motions, respectively. Next, the intensity of the input motions was increased in stages from small to large. The sequence of the dynamic loading and the number of input earthquakes applied to each test model are listed in Table 3.

The frequency characteristics of the soil and structure are significant to determine the dynamic behavior of the soil-foundation-structure system during earthquakes. Figure 5 shows the ratio of response spectrum (RRS) of the soil surface and each structural model (ST4, 8, and 12) during the weak sweep signal. To observe the natural period of soil, the RRS between the soil surface and bedrock motion was observed. From the RRS, the natural period of the soil was approximately 0.18 s. The natural period of the structure considering SFSI was also obtained from the RRS between the structure and soil surface motion. The natural period of ST4, ST8, and ST12 from the RRS was 0.2, 0.37, and 0.58 s, respectively. Since the natural period of the structure from the RRS includes the foundation behavior, the natural period of the structure was lengthened compared with the value obtained from the impact hammer tests.

4 Test results

4.1 Backbone curve development from slow cyclic and dynamic tests

Figure 6 depicts the rotated SDOF structure during slow cyclic and dynamic tests. In the slow cyclic test (Fig. 6a), when the foundation–structure was subjected to cyclic loading, the foundation was subjected to overturning moment due to the horizontal force (F) as well as the self-weight of the superstructure (W). The overturning moment of the foundation (M_o) during the slow cyclic tests is expressed as (Gajan and Kutter 2008)

$$M_o = F \cdot \left(h_{act} + s\right) + W \cdot h(\sin\theta) \tag{5}$$

where h_{act} is the height of the cyclic loading point, s is the foundation settlement, $W = m_s g$ (g is the gravitational acceleration), and θ is the foundation rotation angle.

In most studies, the dynamic overturning moment of the foundation was determined based on the total acceleration of the superstructure. Gajan and Kutter (2008) determined the overturning moment from the free body diagram of the shear wall structure and stated that the horizontal acceleration of the shear wall structure mostly contributes to the dynamic overturning moment of the foundation. In addition, Anastasopoulos et al. (2013) and Tsatsis and Anastasopoulos (2015) determined the critical acceleration of the superstructure (a_c), the maximum acceleration of the superstructure, based on the ultimate moment capacity of the foundation.

$$a_c = M_{ult}/m_s h \Leftrightarrow M_{ult} = m_s \cdot a_c \cdot h. \tag{6}$$

Based on previous studies, this study determined the dynamic overturning moment of the foundation as follows (Fig. 6b):

$$M_o = m_s \cdot a_s \cdot h \tag{7}$$

where a_s is the horizontal acceleration of the superstructure.

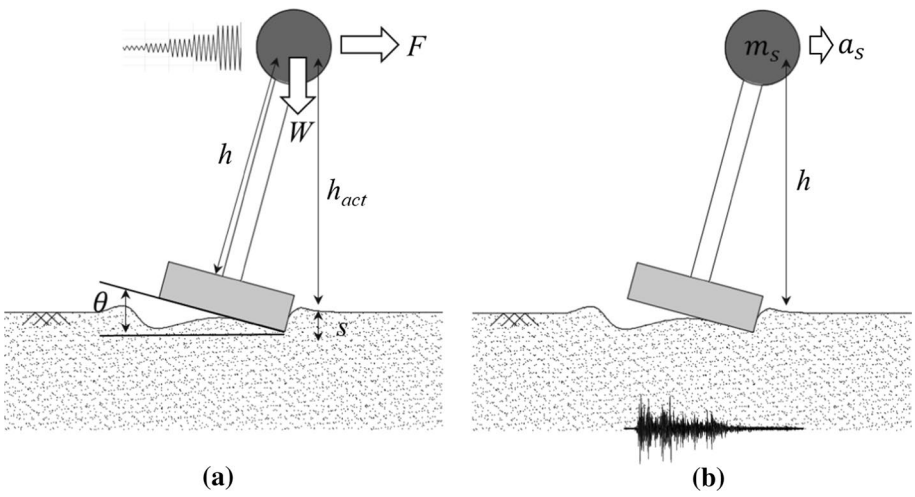

Fig. 6 Illustration of rocking behavior of SDOF structure for determining the overturning moment of the foundation: **a** slow cyclic tests; **b** dynamic tests

To reflect the directional behaviors of rocking motion, the representative values of the overturning moment and foundation rotation angle for each loop and events of the slow cyclic and dynamic tests, respectively were decided as a point of the average values (Fig. 7). The average values of the overturning moment (M_{avg}) and rotation (θ_{avg}) used to develop the backbone curve were determined using the following equations.

$$M_{avg} = \frac{1}{2}\left(M_{max} + \left|M_{min}\right|\right) \tag{8}$$

$$\theta_{avg} = \frac{1}{2}\left(\theta_{max} + \left|\theta_{min}\right|\right) \tag{9}$$

where M_{max} and θ_{max} are the maximum moment and the maximum rotation of the foundation, respectively, M_{min} and θ_{min} are the minimum moment and the minimum rotation of the foundation, respectively.

Using the average moment and rotation of each cycle in the slow cyclic tests, the hyperbolic fitting method for the moment–rotation relation was used to develop the backbone curve, and the general formulas of the fitting curve is expressed as,

$$M_o = \frac{\theta}{\frac{1}{a} + \frac{\theta}{b}} \tag{10}$$

where a and b are numerical coefficients.

Figure 8 shows the overturning moment–rotation relation of ST8 (i.e., backbone curve: slow cyclic tests; hysteresis loop: dynamic tests, Ofunato and Hachinohe at the initial virgin stage). As shown in the figure, the dynamic moment–rotation relation did not match the slow cyclic moment–rotation relation, and the overturning moment–rotation hysteresis loop of the dynamic test was much stiffer than the slow cyclic backbone curve regardless of the type of input earthquake. Moreover, a large difference occurred at a large rotation, and this phenomenon can be clearly observed in Fig. 9, which depict the average dynamic overturning moment–rotation of each input motion as a point (i.e., Eqs. 8, 9, and Fig. 7). During the dynamic tests, a strong earthquake caused a large rotation of the foundation and a large structural bending owing to the relation between the excitation frequency and the natural period of the structure. Consequently, there was a difference in the dynamic

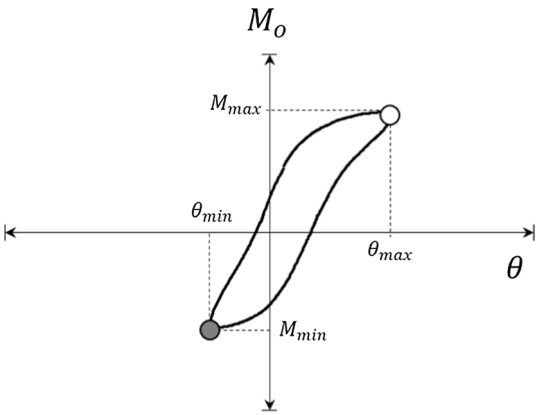

Fig. 7 Moment–rotation hysteresis loop to define the average moment

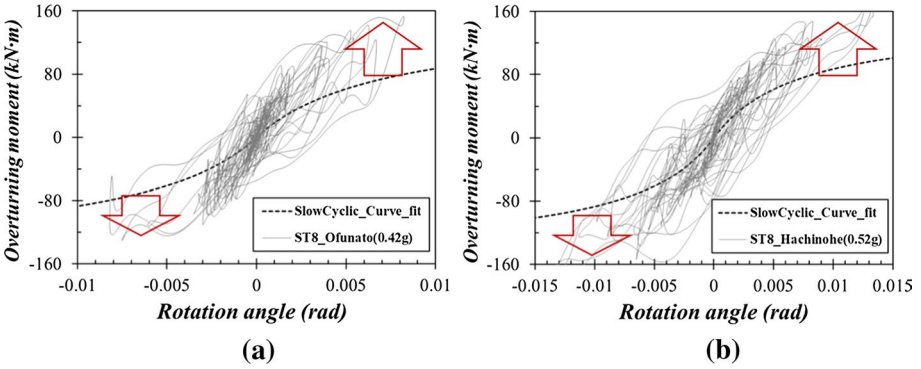

Fig. 8 Backbone curve of the slow cyclic tests and hysteresis loop for ST8 model: **a** ofunato at the initial virgin stage (surface PGA: 0.42 g); **b** Hachinohe at the initial virgin stage (surface PGA: 0.52 g)

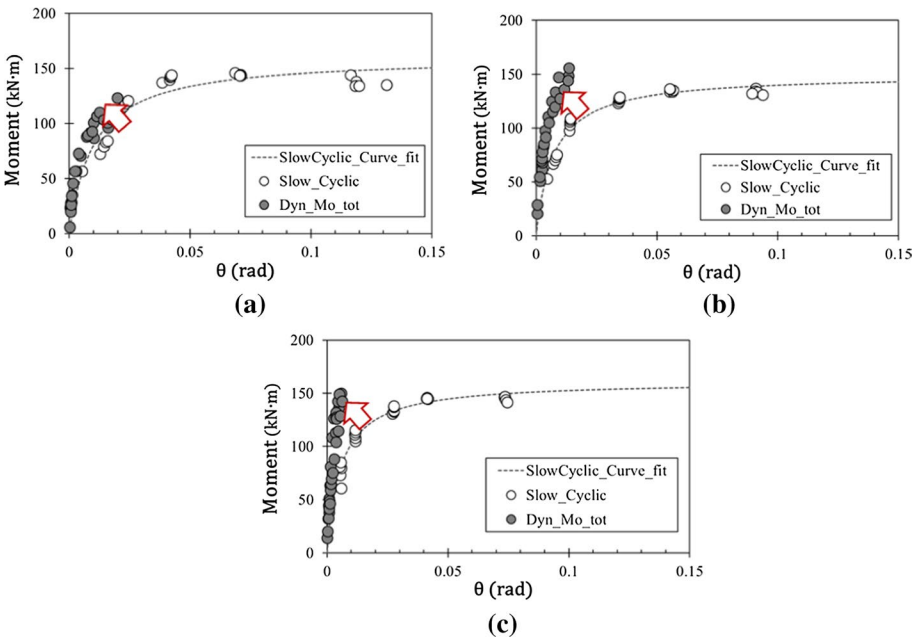

Fig. 9 Comparison of moment rotation backbone curve of the slow cyclic tests and dynamic moment rotation relation: **a** ST4; **b** ST8; **c** ST12

rocking behavior determined by the total acceleration of the structure and the slow cyclic rocking behavior, especially at a large rotation, due to structural bending. Structural bending affected not only the difference in the overturning moment between the slow cyclic and dynamic tests, but also the dynamic foundation rotation between test models, ST4, ST8, and ST12.

The crucial point determining the structural bending during the same earthquake loading is the natural period of the structure calculated by the effective mass and stiffness of

the structure. However, the difference in the effective mass of the structural models in this study is not large, so that the structural bending motion during earthquake is mostly affected by the structural stiffness. The phenomena are discussed in subsequent sections.

4.2 Effect of structural stiffness on foundation rocking behavior

Gajan and Kutter (2009b) showed that the slenderness ratio (moment-to-shear ratio) determines the dominant behavior of foundation motion such as sliding and rocking for a rigid oscillator and the system. A system with a slenderness ratio greater than 1 exhibits dominant rocking behavior during dynamic motion. In addition, a system with a larger slenderness ratio presents a larger rotation angle during dynamic behavior. However, as shown in Fig. 9a, ST4, which had a smaller slenderness ratio than ST8 and ST12, had a larger rotation. In case of a rigid oscillator, the rotation of the foundation–structure system generally increases with the slenderness ratio during dynamic loading. However, when structural stiffness was considered, it was not always true that the rotation of the foundation–structure system increased with the slenderness ratio since the height of the structure (h) directly affects the structural stiffness (k_s). The structural stiffness is inversely proportional to the effective height of the structure as indicated below.

$$k_s \propto EI/h^3 \tag{11}$$

where E is the Young's modulus of the structure, and I is the second moment of inertia. It indicates that if the foundation length is the same, increasing the height of the structure increases the slenderness ratio of the system, and eventually, the rocking behavior of the foundation increases, while the structural stiffness decreases. On the other hand, Heron et al. (2013) stated that if the slenderness ratio of the system is the same, a structure with a larger structural stiffness would generate a larger rotation than a structure with a relatively smaller structural stiffness. Consequently, the effect of the structural stiffness and height interact with each other and should be considered, simultaneously. This phenomenon is clearly observed in Fig. 10.

Figure 10 shows the peak rotation angle of the foundation and the structural net displacement of each dynamic event with peak ground acceleration (PGA) at the soil surface for ST4 and ST12. As shown in Fig. 10, the rotation angle and the structural net displacement increased with surface PGA since a strong ground motion generated a large deformation on the foundation–structure system. In general, the maximum structural net

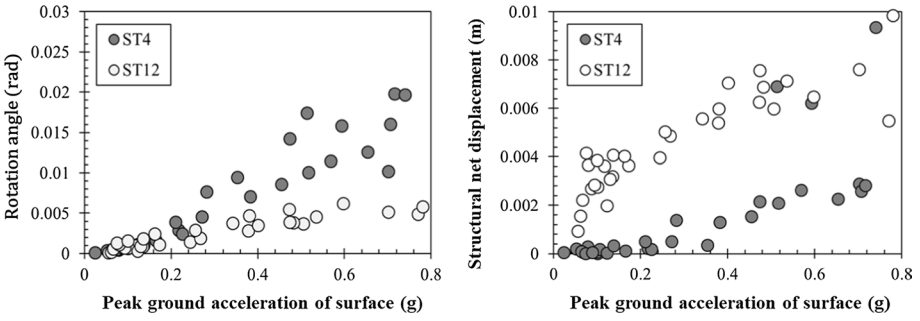

Fig. 10 Maximum foundation rotation angle and maximum structural net displacement with peak ground acceleration of soil surface

displacement of ST12 was larger than that of ST4 with PGA at the surface; for the maximum rotation angle, the opposite situation occurred regardless of the type of the input earthquake. When the inertial force is applied to the structure, a structure with a lower structural stiffness dissipates seismic energy through the structure itself due to bending of the structure, so that the rotation angle of the foundation is small. On the other hand, a structure with a larger stiffness has a larger rotation because seismic energy is dissipated by the rocking behavior of the foundation and not by structural motion (Heron et al. 2013).

In the case of ST4 and ST12, the effect of the structural stiffness on the foundation rocking behavior seemed to be greater than the effect of the slenderness ratio; phase difference analysis in the time domain for each testing model is discussed in the following section by considering the structural stiffness.

4.3 Phase difference of foundation rocking, sliding, and structural net displacement in the time domain

The total horizontal displacement of the structure was decomposed into structural net displacement, foundation horizontal motion, and horizontal displacement owing to foundation rocking (i.e., $u_{tot.} = u_{net} + u_f + u_\theta h$). Figure 11 shows the time history of the structural displacement decomposed into three parts for strong earthquake (Hachinohe, surface PGA: 0.78 g). To observe the phase difference of each of the three parts, the range, when the strongest seismic shaking was inputted, was enlarged. During the earthquake, the foundation first moved horizontally regardless of the structural stiffness. Since the foundation was embedded for all test models, the foundation and soil moved together. Next, the foundation–structure rotation and structural bending occurred. As shown in Fig. 11, horizontal displacement due to foundation rocking of ST4 and ST12 was almost in phase with the structural net displacement. Owing to this effect, the foundation rocking behavior can reduce the structural seismic response; this is known as the rocking effect (Kim et al. 2015). However, the relation between the foundation horizontal motion and the structural net motion exhibited different behaviors depending on the structural stiffness. In the case of ST4, the structural net displacement directly followed the foundation horizontal motion owing to the large structural effective stiffness during the early part of seismic shaking (12–14 s). Moreover, during strong seismic shaking (16–17 s), the structural net displacement followed the foundation horizontal motion. In contrast, ST12 showed a different behavior. Although the horizontal motion due to foundation rocking was in phase with the structural net displacement, the foundation horizontal motion was out of phase with the structural net displacement throughout shaking. Since the effective stiffness of ST12 was much smaller than that of ST4, the structural net displacement of ST12 could not follow the foundation horizontal motion directly.

To quantify the phase difference in the time domain between the two foundation motions (horizontal motion and horizontal displacement due to rocking) with respect to the structural net displacement, the local time delay of each motion was evaluated. Figure 12a shows the definition of local time delay based on structural net motion. For instance, the time for the peak amplitude of foundation horizontal motion subtracted from the time for the peak amplitude of the structural net displacement is the local time delay of foundation horizontal motion. As shown in Fig. 12b–d, the local time delay of foundation rocking was approximately close to zero regardless of the test model. This indicates that foundation rocking and structural net displacement were in phase during the earthquake. In addition, most local time delays of foundation horizontal motion were positive since the foundation

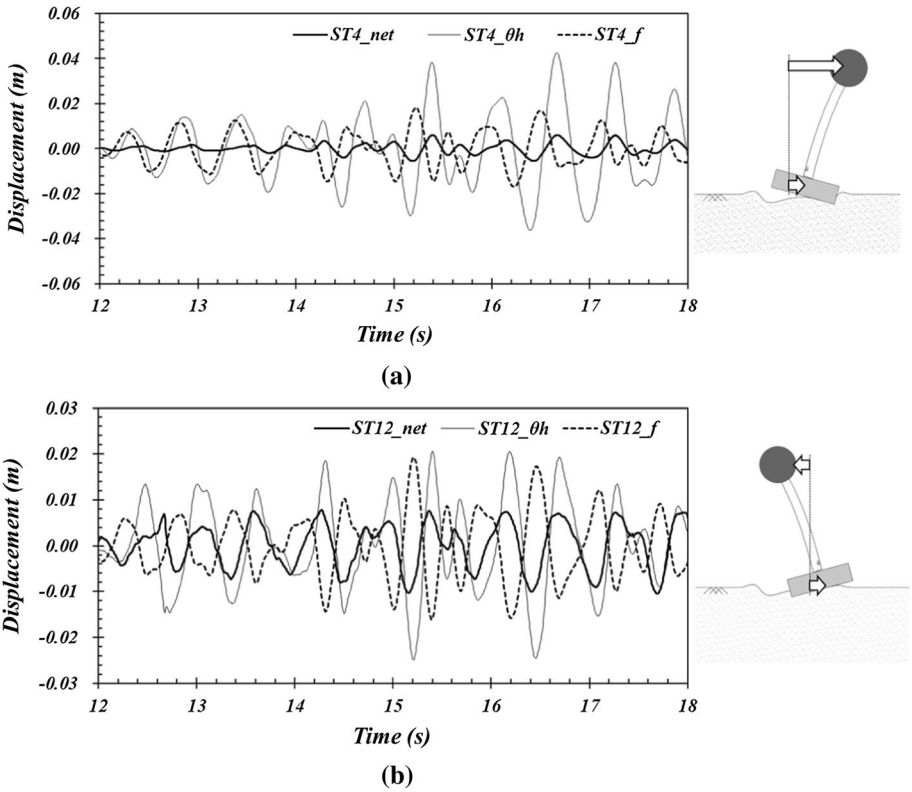

Fig. 11 Time history of structural displacement decomposed into structural net displacement (u_{net}), foundation rotation ($\theta \cdot h$), and foundation displacement (u_f) for strong earthquake (Hachinohe, surface PGA: 0.78 g): **a** ST4; **b** ST12

horizontal motion moved horizontally first when the earthquake load was applied. However, the values of the local time delay of foundation horizontal motion were different depending on the test model. As previously discussed, while the foundation horizontal motion of ST4 with a larger structural effective stiffness was in phase with the structural net displacement, the local time delays of foundation horizontal motion for ST8 and ST12 with smaller structural effective stiffness values than ST4 were much larger than that of ST4. Thus far, the extent of the difference in the structural dynamic response depending on structural stiffness has been examined. Therefore, the following section will discuss how to reflect the structural stiffness to the dynamic overturning moment.

4.4 Re-evaluation of dynamic overturning moment of the foundation considering structural bending

The total horizontal displacement of the structure (u_{tot}) was decomposed into foundation horizontal (u_f), foundation rocking (θh), and structural net displacement (u_{net}). Since the dynamic overturning moment of the foundation is governed by the maximum motion of the structure, the portion of each decomposed motion at the maximum motion of the structure is important in order to consider structural bending. Therefore, to observe the portion of

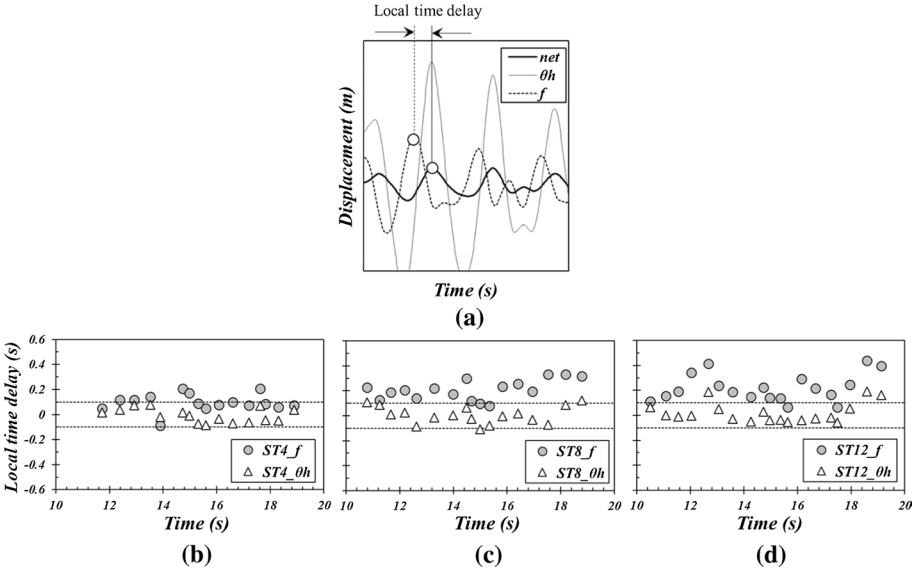

Fig. 12 Local time delay based on structural net displacement in the time domain for strong earthquake (Hachinohe, surface PGA: 0.78 g): **a** definition of local time delay; **b** ST4; **c** ST8; **d** ST12

the structural net displacement at maximum displacement of the structural total motion for each dynamic event, the horizontal displacement due to foundation motion (i.e., $u_f + \theta h$) and the structural net displacement (u_{net}) are presented for each dynamic event (Fig. 13). In the case of ST4, the horizontal displacement due to the foundation was almost located on a 1:1 line with the maximum total displacement of the structure. This indicates that most of the structural total displacement was determined by foundation motion and the foundation behavior was dominant rather than the structural net motion due to large structural effective stiffness. For the ST8 and ST12, the foundation behavior (i.e., $u_f + \theta h$) was larger than the structural net motion (u_{net}) at large total displacement. However, the structural net displacements of ST8 and ST12 had larger portions of maximum total displacement of the structure than that of ST4 owing to a more flexible structure.

As shown in Fig. 14, the ratio of the foundation motion and the structural net displacement was observed at maximum total structural horizontal displacement. The ratio of the foundation motion (R_f) and the structural net motion (R_{net}) are expressed as:

$$R_f = \left| \frac{\left(u_f + \theta \cdot h\right)}{u_{tot}} \right| \tag{12}$$

$$R_{net} = \left| \frac{u_{net}}{u_{tot}} \right| \tag{13}$$

These results clearly show the difference between foundation and structural net behaviors. In the case of ST4, the foundation behavior was dominant even when the total displacement of the structure was small. In contrast, for the ST8 and ST12, when the total

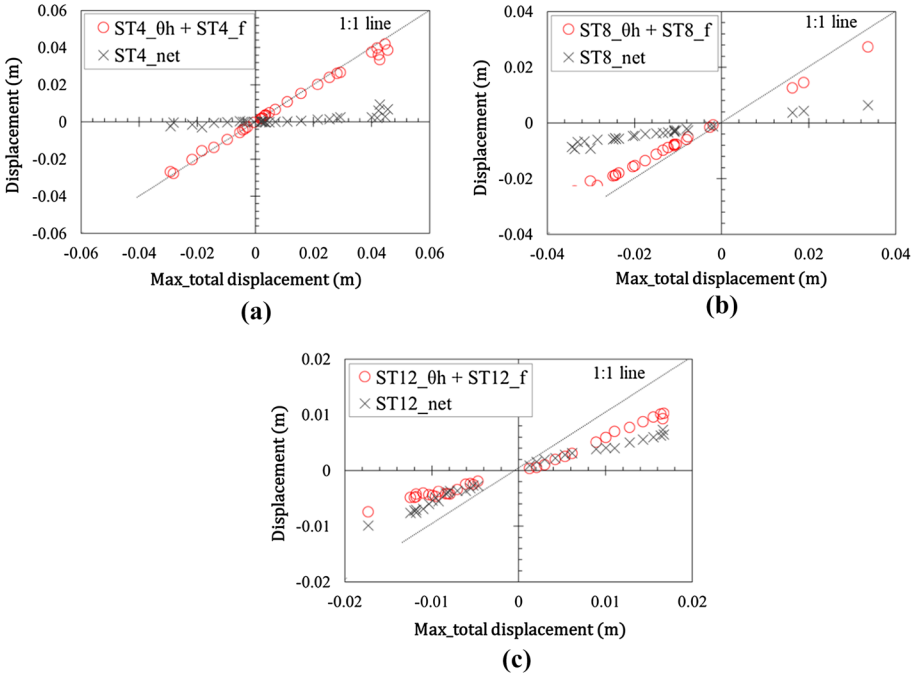

Fig. 13 Decomposition of structural total displacement (u_{tot}) into foundation displacement ($u_f + \theta \cdot h$) and structural net displacement (u_{net}) with maximum horizontal displacement of structural total motion for each seismic shaking: **a** ST4; **b** ST8; **c** ST12

displacement of the structure was small, the net structural motion was dominant rather than the foundation motion. However, as the total displacement of the structure increases, the foundation motion increases and the contribution of the two motions becomes similar.

To evaluate the dynamic overturning moment of the foundation by considering structural bending, the dynamic overturning moment calculated using Eq. 7 was re-evaluated. As previously discussed, the ratio of the structural net motion (R_{net}) was different depending on the structural effective stiffness, and ST4, which had a larger effective stiffness, showed a much smaller ratio of the structural net motion (R_{net}) than ST8 and ST12. Therefore, the dynamic overturning moment calculated using Eq. 7 was not significantly different from the moment rotation backbone results of the slow cyclic test results. However, in the case of ST8 and ST12, since the ratio of the structural net motion was much larger than that of ST4, there was a significant difference between the slow cyclic and dynamic rocking behaviors in the moment–rotation curve. Consequently, the structural bending motion produced the difference between the slow cyclic and dynamic rocking behaviors, and the dynamic overturning moment was re-evaluated by considering structural bending as follows:

$$M_{o\_revise} = M_o \cdot \left(1 - R_{net}\right) = M_o \cdot \left(1 - \left|\frac{u_{net}}{u_{tot}}\right|\right) = m_s \cdot a_s \cdot h \cdot R_f \tag{14}$$

where M_{o_revise} is the re-evaluated dynamic overturning moment. As shown in Fig. 15, although the dynamic overturning moment calculated using Eq. 7 did not match the slow

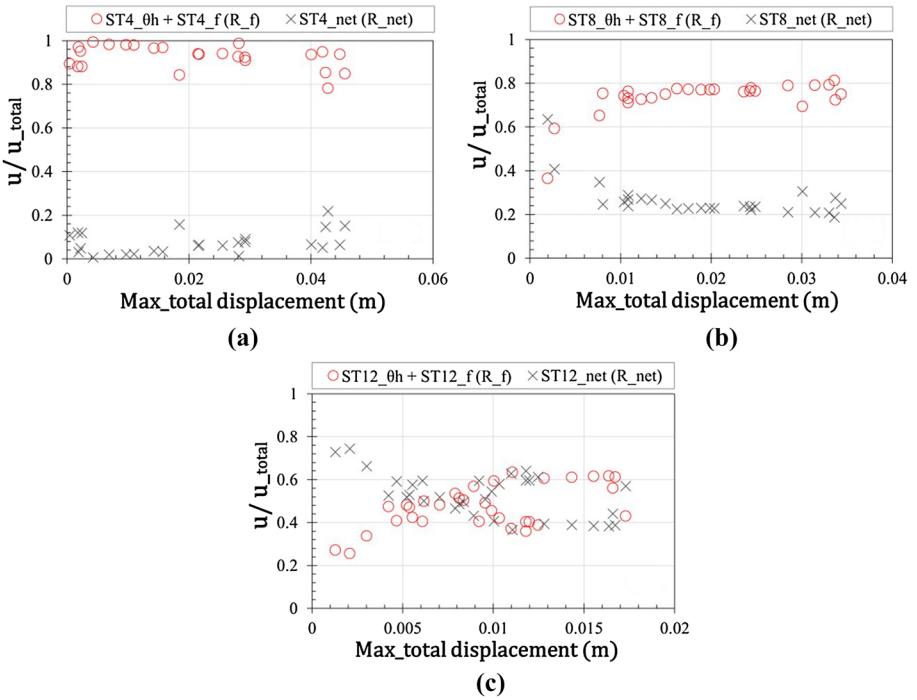

Fig. 14 Ratio of foundation motion (R_f) and structural net displacement (R_{net}) at maximum horizontal displacement of structural total motion for each dynamic event: **a** ST4; **b** ST8; **c** ST12

cyclic backbone curves, the re-evaluated dynamic overturning moment closely matched the slow cyclic backbone curves. Therefore, to compare the slow cyclic and dynamic rocking behaviors, the structural bending should be considered.

5 Conclusions

Nowadays, several studies have been conducted on rocking foundation based on the slow cyclic and dynamic tests by assuming the structure as a rigid oscillator. However, when structural bending is included, the rocking behaviors of the foundation obtained from the slow cyclic and dynamic tests are different. Therefore, a clear description of each method and how each behavior is different should be investigated by considering structural bending. To fill the gap between the cyclic and dynamic rocking behaviors, embedded foundation models with various slenderness ratios of the systems were investigated using horizontal slow cyclic tests and dynamic tests in a centrifuge. To simulate the structure and foundation conditions in practice, the foundation was embedded and the range of the slenderness ratio of the systems was 1–2. From the test results, the rocking behavior of the foundation was affected by structural bending. The overturning moment in the dynamic test determined by the conventional method was different compared with results from the slow cyclic test due to the structural bending motion. Finally, the overturning moment was re-evaluated by considering structural bending, and the re-evaluated dynamic overturning

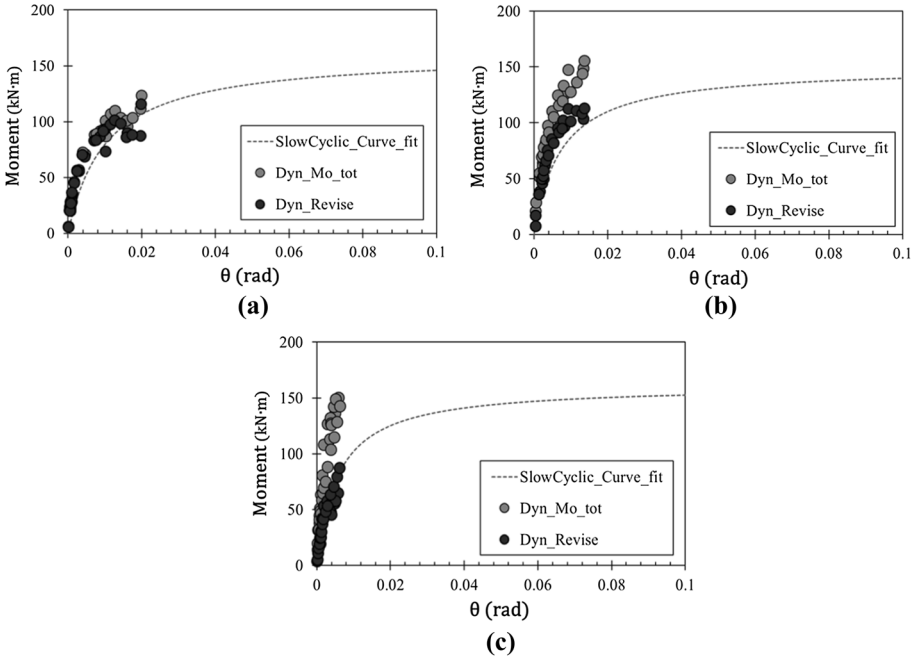

Fig. 15 Comparison of moment–rotation backbone curve of the slow cyclic tests and the re-evaluated dynamic moment rotation relation: **a** ST4; **b** ST8; **c** ST12

moment matched the results from the slow cyclic tests. The important findings from this study are summarized below.

1. The dynamic structural response includes both the foundation and structural bending motions. In the slow cyclic tests, the structural bending motion would not be significant due to the longer period of loading compared with the natural period to the structure. Therefore, when the structure is not a rigid oscillator, the dynamic overturning moment without considering structural bending cannot be directly compared with results of the slow cyclic test.
2. During seismic shaking, the structural net displacement had different characteristics depending on the structural effective stiffness. When seismic load was applied, foundation horizontal motion first responded, and the structural bending motion was almost in phase with the foundation rocking behavior. The structural bending motion of ST4, which had a large effective stiffness, closely followed the foundation horizontal motion, while those of ST8 and ST12, with smaller effective stiffness values than ST4, were out of phase.
3. From the evaluation of structural bending motion, it was shown that the structural net displacement generates the difference between the slow cyclic and the dynamic overturning moment of the foundation. By excluding the structural bending motion from the dynamic overturning moment, the dynamic overturning moment of the foundation was re-evaluated. Finally, by comparing the overturning moment from the slow cyclic and

the re-evaluated dynamic tests, a closely-matched moment–rotation curve of the slow cyclic and dynamic rocking behaviors was developed.

The following are the limitations of this study.

1. The dynamic centrifuge tests in this study was based on stage tests. The effect of soil densification during the dynamic centrifuge tests will affect the dynamic behavior of the foundation-structure system due to the loose soil with a relative density of 40%. Although the natural period of the soil was described, in the future, it is also necessary to consider the influence of soil densification during the stage tests.
2. This study described the effect of structural stiffness on the rocking behavior of the foundation. However, the structural models investigated had varying slenderness ratios of the system, as well as varying structural stiffnesses. Therefore, to isolate the effect of structural stiffness and slenderness ratio on the rocking behavior of the foundation, it is necessary to conduct the tests with structures that have the same height and varying structural stiffnesses.

Acknowledgements This work was supported by the National Research Foundation of Korea (NRF) grant funded by the Korea government (MSIT) (No. NRF-2015R1A2A1A15054531, No. 2017R1A5A1014883). The authors would like to thank Prof. Hyung-Jo Jung for his advice, as well as to the staff of the Centrifuge facility of KAIST (Mr. Seungbok Lee and Mr. Kyeongsik Seo).

References

Allmond JD, Kutter BL (2014) Design considerations for rocking foundations on unattached piles. J Geotech Geoenviron Eng 140(10):04014058. https://doi.org/10.1061/(ASCE)GT.1943-5606.0001162

Anastasopoulos I, Gazetas G, Loli M, Apostolou M, Gerolymos N (2010) Soil failure can be used for seismic protection of structures. Bull Earthq Eng 8(2):309–326

Anastasopoulos I, Gelagoti F, Kourkoulis R, Gazetas G (2011) Simplified constitutive model for simulation of cyclic response of shallow foundations: validation against laboratory tests. J Geotech Geoenviron Eng 137(12):1154–1168

Anastasopoulos I, Kourkoulis R, Gelagoti F, Papadopoulos E (2012) Rocking response of SDOF systems on shallow improved sand: an experimental study. Soil Dyn Earthq Eng 40:15–33

Anastasopoulos I, Loli M, Georgarakos T, Drosos V (2013) Shaking table testing of rocking-isolated bridge pier on sand. J Earthq Eng 17(1):1–32

Anastasopoulos I, Gelagoti F, Spyridaki A, Sideri J, Gazetas G (2014) Seismic rocking isolation of an asymmetric frame on spread footings. J Geotech Geoenviron Eng 140(1):133–151

Combescure D, Chaudat T (2000) ICONS European program seismic tests on R/C walls with uplift; CAMUS IV specimen. ICONS Project, CEA/DRN/DMT, Report SEMT/EMSI/RT/00-27/4

Deng L, Kutter BL (2012) Characterization of rocking shallow foundations using centrifuge model tests. Earthq Eng Struct Dyn 41(5):1043–1060

Deng L, Kutter BL, Kunnath SK (2012) Centrifuge modeling of bridge systems designed for rocking foundations. J Geotech Geoenviron Eng 138(3):335–344

Deng L, Kutter BL, Kunnath SK (2014) Seismic design of rocking shallow foundations: displacement-based methodology. J Bridge Eng 19:04014043. https://doi.org/10.1061/(ASCE)BE.1943-5592.0000616

Drosos V, Georgarakos T, Loli M, Anastasopoulos I, Zarzouras O, Gazetas G (2012) Soil-foundation-structure interaction with mobilization of bearing capacity: experimental study on sand. J Geotech Geoenviron Eng 138(11):1369–1386

Figini R, Paolucci R (2017) Integrated foundation–structure seismic assessment through non-linear dynamic analyses. Earthq Eng Struct Dyn 46(3):349–367

Fukui J, Kimura Y, Ishida M, Kishi Y (1999) An investigation on the response of shallow foundations to large earthquakes. No. 3627, Technical Memorandum of PWRI, Tsukuba

Gajan S, Kutter BL (2008) Capacity, settlement, and energy dissipation of shallow footings subjected to rocking. J Geotech Geoenviron Eng 134(8):1129–1141

Gajan S, Kutter BL (2009a) Contact interface model for shallow foundations subjected to combined cyclic loading. J Geotech Geoenviron Eng 135(3):407–419

Gajan S, Kutter BL (2009b) Effects of moment-to-shear ratio on combined cyclic load-displacement behavior of shallow foundations from centrifuge experiments. J Geotech Geoenviron Eng 135(8):1044–1055

Gajan S, Kutter BL, Phalen JD, Hutchinson TC, Martin GR (2005) Centrifuge modeling of load-deformation behavior of rocking shallow foundations. Soil Dyn Earthq Eng 25(7):773–783

Gazetas G (2015) 4th Ishihara lecture: soil–foundation–structure systems beyond conventional seismic failure thresholds. Soil Dyn Earthq Eng 68:23–39

Gazetas G, Anastasopoulos I, Adamidis O, Kontoroupi T (2013) Nonlinear rocking stiffness of foundations. Soil Dyn Earthq Eng 47:83–91

Gelagoti F, Kourkoulis R, Anastasopoulos I, Gazetas G (2012) Rocking isolation of low-rise frame structures founded on isolated footings. Earthq Eng Struct Dyn 41(7):1177–1197

Hakhamaneshi M, Kutter BL (2016) Effect of footing shape and embedment on the settlement, recentering, and energy dissipation of shallow footings subjected to rocking. J Geotech Geoenviron Eng 142(12):04016070. https://doi.org/10.1061/(ASCE)GT.1943-5606.0001564

Hakhamaneshi M, Kutter BL, Moore M, Champion C (2016) Validation of ASCE 41-13 modeling parameters and acceptance criteria for rocking shallow foundations. Earthq Spectra 32(2):1121–1140

Heron CM, Haigh SK, Madabhushi SPG (2013) Susceptibility of shallow foundations to rocking and sliding movements during seismic loading. In: Ilki A, Fardis MN (eds) Seismic evaluation and rehabilitation of structures, geotechnical, geological and earthquake engineering, vol 26. Springer, Cham, pp 407–424

Heron CM, Haigh SK, Madabhushi SPG (2015) A new macro-element model encapsulating the dynamic moment-rotation behaviour of raft foundations. Géotechnique 65(5):442–451

Hung HH, Liu KY, Ho TH, Chang KC (2011) An experimental study on the rocking response of bridge piers with spread footing foundations. Earthq Eng Struct Dyn 40(7):749–769

Kim DS, Kim NR, Choo YW, Cho GC (2013a) A newly developed state-of-the-art geotechnical centrifuge in Korea. KSCE J of Civ Eng 17(1):77–84

Kim DS, Lee SH, Choo YW, Perdriat J (2013b) Self-balanced earthquake simulator on centrifuge and dynamic performance verification. KSCE J Civ Eng 17(4):651–661

Kim DK, Lee SH, Kim DS, Choo YW, Park HG (2015) Rocking effect of a mat foundation on the earthquake response of structures. J Geotech Geoenviron Eng 141(1):04014085. https://doi.org/10.1061/(ASCE)GT.1943-5606.0001207

Ko KW, Ha JG, Park HJ, Kim DS (2017) Comparison of rocking behavior between conventional and new-type of shallow foundations via centrifuge tests. In: Proceedings of the 3rd international conference on performance-based design in earthquake geotechnical engineering, Vancouver, Canada

Ko KW, Ha JG, Park HJ, Kim DS (2018) Soil rounding effect on embedded rocking foundation via horizontal slow cyclic tests. J Geotech Geoenviron Eng 144(3):04018004. https://doi.org/10.1061/(ASCE)GT.1943-5606.0001848

Kokkali P, Anastasopoulos I, Abdoun T, Gazetas G (2014) Static and cyclic rocking on sand: centrifuge versus reduced scale 1 g experiments. Géotechnique 64(11):865–880

Kokkali P, Abdoun T, Anastasopoulos I (2015) Centrifuge modeling of rocking foundations on improved soil. J Geotech Geoenviron Eng 141(10):04015041. https://doi.org/10.1061/(ASCE)GT.1943-5606.0001315

Kutter BL, Moore M, Hakhamaneshi M, Champion C (2016) Rationale for shallow foundation rocking provisions in ASCE 41-13. Earthq Spectra 32(2):1097–1119

Lee SH, Choo YW, Kim DS (2013) Performance of an equivalent shear beam (ESB) model container for dynamic geotechnical centrifuge tests. Soil Dyn Earthq Eng 44:102–114

Liu W, Hutchinson TC, Kutter BL, Hakhamaneshi M, Aschheim MA, Kunnath SK (2013) Demonstration of compatible yielding between soil-foundation and superstructure components. J Struct Eng 139(8):1408–1420

Liu W, Hutchinson TC, Kutter BL, Gavras AG, Hakhamaneshi M (2015a) Effect of earthquake-induced axial load fluctuations on asymmetric frame–wall–rocking foundation systems. Earthq Eng Struct Dyn 44(12):1997–2013

Liu W, Hutchinson TC, Gavras AG, Kutter BL, Hakhamaneshi M (2015b) Seismic behavior of frame-wall-rocking foundation systems. I: test program and slow cyclic results. J Struct Eng 141(12):04015059. https://doi.org/10.1061/(ASCE)ST.1943-541X.0001264

Liu W, Hutchinson TC, Gavras AG, Kutter BL, Hakhamaneshi M (2015c) Seismic behavior of frame-wall-rocking foundation systems. II: dynamic test phase. J Struct Eng 141(12):04015060. https://doi.org/10.1061/(ASCE)ST.1943-541X.0001313

Madabhushi G (2014) Centrifuge modelling for civil engineers. CRC Press, Boca Raton

Mergos PE, Kawashima K (2005) Rocking isolation of a typical bridge pier on spread foundation. J Earthq Eng 9(2):395–414

Meyerhof GG (1963) Some recent research on the bearing capacity of foundations. Canadian Geotech J 1(1):16–26

Negro P, Paolucci R, Pedretti S, Faccioli E (2000) Large-scale soil-structure interaction experiments on sand under cyclic loading. In: 12th world conference on earthquake engineering, Auckland New Zealand, New Zealand Society for Earthquake Engineering, Wellington

Panagiotidou AI, Gazetas G, Gerolymos N (2012) Pushover and seismic response of foundations on stiff clay: analysis with p-delta effects. Earthq Spectra 28(4):1589–1618

Paolucci R, Shirato M, Yilmaz MT (2008) Seismic behaviour of shallow foundations: shaking table experiments vs numerical modelling. Earthq Eng Struct Dyn 37(4):577–595

Paolucci R, Figini R, Petrini L (2013) Introducing dynamic nonlinear soil-foundation-structure interaction effects in displacement-based seismic design. Earthq Spectra 29(2):475–496

Pecker A, Paolucci R, Chatzigogos C, Correia AA, Figini R (2014) The role of non-linear dynamic soil-foundation interaction on the seismic response of structures. Bull Earthq Eng 12(3):1157–1176

Pelekis I, Madabhushi GSP, Dejong MJA (2017) Centrifuge investigation of two different soil-structure systems with rocking and sliding on dense sand. In: 6th ECCOMAS thematic conference on computational methods in structural dynamics and earthquake engineering, Rhodes Island Greece. European community on computational methods in applied sciences, Barcelona

Shirato M, Kouno T, Asai R, Nakatani S, Fukui J, Paolucci R (2008) Large-scale experiments on nonlinear behavior of shallow foundations subjected to strong earthquakes. Soils Found 48(5):673–692

Tileylioglu S, Stewart JP, Nigbor RL (2011) Dynamic stiffness and damping of a shallow foundation from forced vibration of a field test structure. J Geotech Geoenviron Eng 137(4):344–353

Tsatsis A, Anastasopoulos I (2015) Performance of rocking systems on shallow improved sand: shaking table testing. Front Built Environ. https://doi.org/10.3389/fbuil.2015.00009